The place-cell representation of volumetric space in rats

Roddy M. Grieves[1]*, Selim Jedidi-Ayoub[1], Karyna Mishchanchuk[1], Anyi Liu[1], Sophie Renaudineau[1] and Kate J. Jeffery[1]*

[1]University College London, Institute of Behavioral Neuroscience, Department of Experimental Psychology, London, United Kingdom

*For correspondence:
r.grieves@ucl.ac.uk (RMG)
k.jeffery@ucl.ac.uk (KJJ)

Abstract

Place cells are spatially modulated neurons found in the hippocampus that underlie spatial memory and navigation: how these neurons represent 3D space is largely unknown. We wirelessly recorded place cells in rats at they explored a cubic lattice climbing frame which could be aligned or tilted with respect to gravity. Place cells represented the entire volume of the mazes: the activity of these cells tended to be aligned with the maze axes, and when it was more difficult for the animals to move vertically the cells represented space less accurately and less stably. These results demonstrate that surface dwelling animals also represent 3D space and suggests there is a fundamental relationship between environment structure, gravity, movement and spatial memory.

Introduction

Place cells are neurons in the hippocampus that fire when an animal visits specific regions of its environment, called place fields, and are thought to provide the foundation for an internal representation of space, or 'cognitive map' (1, 2). The question arises as to whether this map is three-dimensional, and if so whether the properties are the same in all dimensions (3–5). This is important not just for spatial mapping *per se* but also because the spatial map may form the framework for other types of cognition in which information dimensionality is higher than in real space. Understanding how the brain integrates information across dimensions is thus of theoretical importance.

A longstanding question concerns whether this map represents three-dimensional space or whether it is essentially flat, with reduced information about the vertical dimension. A previous study of place cells in rats (6) found vertical elongation of the place fields when rats climbed either a pegboard wall studded with footholds or a spiral track, suggesting that perhaps the cognitive map has a lower resolution for vertical space than for horizontal space (i.e., is anisotropic). This finding was supported by observations that entorhinal grid cells, thought to provide a spatial metric for place cells, showed absent spatial processing in the vertical dimension. However, in a more recent experiment, when rats climbed a wall covered with chicken wire place cells were found to have normally shaped firing fields, although fields themselves occurred with lower probability than on the floor (7). This meant that although the firing of spatial neurons differed between the floor and the wall, the horizontal and vertical components of firing on the wall did not appreciably differ. Taking these findings together, it seems that the differences in spatial encoding previously seen in the vertical dimension may be due to the different constraints on movement, or the locomotor 'affordances' in the different dimensions (8). Meanwhile, a study of flying bats found that place fields did not deviate statistically from spherical (9), suggesting a spatial map of equal resolution in all dimensions (isotropic).

The difference from the rat findings could be due either to the ecological requirements of the species and their differential need for a volumetric map. Alternatively, it could be because the environmental affordance for flight is similar in horizontal vs. vertical dimensions whereas for surface travel the affordances in different dimensions differ. The present experiment aimed to untangle these issues by exploring, in rats, the interaction between gravity, which is what distinguishes horizontal from vertical, and the locomotor affordances of the environment. Animals were recorded using digital telemetry as they explored a volumetric space – an open cubic lattice – through which they could move freely and which had equal properties in all three spatial dimensions. Place cells exhibited firing fields throughout this volume, confirming that these cells underlie a fully three-dimensional volumetric representation of space. Furthermore, we found that place fields tended to be elongated along the axes of the maze (the directions aligned with the boundaries, and in which travel was easiest) with greater elongation for the vertical axis and a resultant lower spatial information and decoding accuracy. We then tilted the lattice so that the three planes of movement all had the same relationship to gravity, and were thus all equally easy (or hard) to traverse. We found that the elongation of the axes followed the tilt of the maze, and the difference between horizontal and vertical place field metrics disappeared. Thus, it seems that differences between horizontal and vertical metrics in spatial encoding arise from the greater movement constraints (lower locomotor affordance, resulting in and greater effort and lower movement time in that dimension) for vertical than horizontal travel, rather than from an intrinsic difference in resolution between directions aligned with vs. orthogonal to gravity. These findings suggest that locomotor affordances in the environment, of which gravity is one modulator, have an effect on encoding structure and accuracy of the spatial map. This may have implications for spatial mapping not just in vertical space, but in any space in which locomotion is difficult or interrupted.

Results

Rats explored the lattice maze fully, but adopted a layer strategy

Rats explored the lattice mazes (Fig. S1) fully, with slightly more coverage in the aligned than the tilted configuration (Fig. S2A-B). In both configurations they spent more time in the lower half, and remained closer to the maze boundaries (Fig. S2C-D). We looked for horizontal movement bias (10) by counting transitions between maze units. In the aligned configuration animals explored the three dimensions differently (median layer transitions/s along X,Y & Z: 0.34, 0.35 & 0.12 Hz, $\chi^2(2) = 14.0$, $p = .0009$, $\eta_p^2 = 0.51$, FT) and post-hoc tests confirmed that they made significantly fewer layer crossings along the (vertical) Z-dimension (X vs Z & Y vs Z, $p < .02$, X vs Y, $p > .99$, Fig. 1A-C). Animals also moved significantly more slowly along the Z-axis of the aligned lattice (Fig. S2E). By contrast, animals moved equivalently along the (now rotated) axes of the tilted lattice, which we labelled A, B and C (Fig. 1C & Fig. S2A).

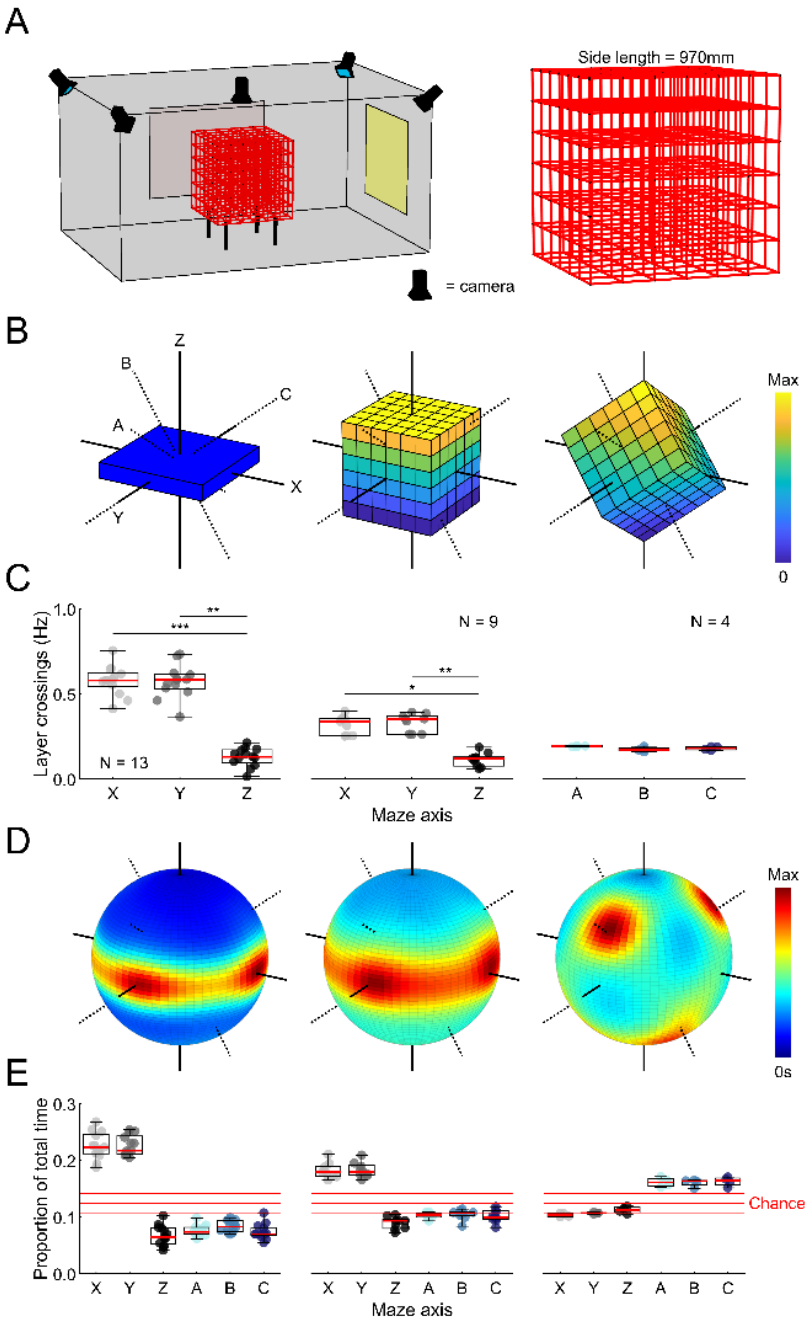

Figure 1: Behavior of animals in the lattice maze. (A) Room and maze (shown in aligned configuration). (B) Schematic of the maze configurations, color-coded to show height. (C) Frequency with which animals crossed between lattice layers in the two configurations. Each marker represents an animal. Note preference for horizontal crossings in the aligned lattice maze. (D) Three-dimensional heat plots of trajectory distribution for the three maze configurations, ordered as in (B) and (C). Note concentration around horizontal trajectories for the arena and aligned maze, and along the three axes for the tilted maze. (E) Each marker represents an animal: graphs show proportion of total session time spent moving roughly parallel to each possible maze axis. Red lines show the 1st 50th and 99th percentile of a shuffle distribution (see Methods).

In the arena, animals' movements were mostly parallel to the horizontal X and Y-axes (median proportion of time along X & Y: 0.22 & 0.22) and their movements were distributed between these two axes equally ($\chi^2(1) = 0.08$, $p = .78$, $\eta_p^2 = 0.001$, FT). In the aligned lattice animals spent more time moving parallel to the X and Y axes than would be expected by chance, but they rarely moved along the other axes (Z, or A, B and C; median proportion of time along A, B, C, X, Y & Z respectively: 0.10, 0.11, 0.10, 0.18, 0.18 & 0.09, chance 97.5th percentile: 0.13). Animals thus travelled along the maze axes significantly differently ($\chi^2(2) = 14.0$, $p = .0009$, $\eta_p^2 = 0.52$, FT) and post-hoc tests confirmed that they explored the X and Y axes similarly, but the Z axis significantly less (X vs Z & Y vs Z, $p < .02$, X vs Y, $p > .99$). This again confirms a strong horizontal bias in their movements when climbing through the lattice (10). Lastly, in the tilted lattice only the A, B and C axes of this maze were traversed more than chance (median proportion of time along A, B, C, X, Y & Z: 0.16, 0.16, 0.16, 0.10, 0.11, 0.11, chance 97.5th percentile: 0.13) and these axes were traversed equally ($\chi^2(2) = 1.5$, $p = .47$, $\eta_p^2 = 0.13$, FT). These effects can be seen in Fig. 1D-E.

Place fields were distributed uniformly throughout the lattices

In total we recorded 756 place cells in the lattice maze environments from 13 rats (Table S2). Representative place cells can be seen in Fig. 2A and Fig. S3. The proportion of active cells (having at least one place field) in the 3D lattice did not differ significantly from in the 2D arena (arena & aligned lattice: 82.5% & 85.2%, $\chi^2(1) = 1.51$, $p = .28$, OR = 0.82; arena & tilted lattice: 82.5% & 83.8%, $\chi^2(1) = 0.18$, $p = .67$, OR = 0.91, Chi-square tests of equal proportions). However, the number of place fields per cell differed between mazes (arena, aligned and tilted median fields/cell: 1.0, 1.0 & 2.0; $\chi^2(2) = 48.63$, $p < .0001$, $\eta_p^2 = .04$, K-W) with cells unsurprisingly exhibiting significantly more fields in the lattice (arena vs aligned & arena vs tilted, $p < .0001$, aligned vs tilted, $p = .29$, Fig. S4A-B). However fields were also more sparse in the lattice [median of 2.21 fields per m^3 in the open field but only

0.69 per m^3 in the aligned configuration and 1.23 per m^3 in the tilted configuration ($\chi^2(2)$ = 781.7, $p < .0001$, $\eta_p^2 = .70$, K-W; arena vs aligned & arena vs tilted, $p < .0001$, aligned vs tilted, $p = .001$, Fig. S4C]. Fields were distributed throughout the lattices uniformly [Fig. 2B-C, GP algorithm (see supplementary methods) aligned observed slope: 2.68, shuffle 95% confidence intervals: 2.65 & 2.79; tilted observed slope: 2.63, shuffle 95% confidence intervals: 2.61 & 2.84] and in each case the median field centroids lay close to the maze center (Fig. S4F).

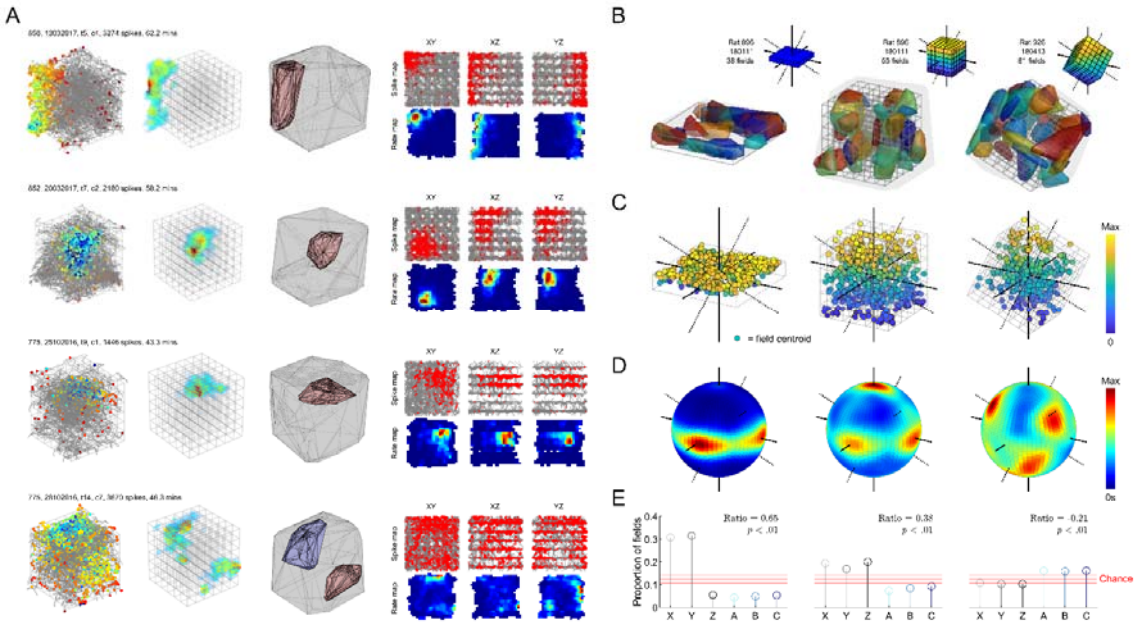

Figure 2: Distribution of place fields in the lattice maze. (*A*) Representative example place cells and their activity in the aligned lattice maze. Four cells are shown, one per row. First column shows the path of the animal and spikes plotted as colored markers. Marker color denotes spike density. Second column shows the three-dimensional firing rate map. Colors denote firing rate and follow the color axis of (D) but areas of low or no firing are transparent. Third column shows the convex hull of the dwell time map as a grey outline and the convex hull of any detected place field(s) as separate (color-coded) polygons. Last column shows the spike and firing rate maps when the data are projected onto the three possible cardinal planes. (*B*) Representative arena, aligned and tilted lattice recording sessions demonstrating homogenous distribution of fields. To allow clearer distinction of separate (color-coded) fields, only fields with a volume less than 300 voxels (one voxel = $50mm^3$) are shown (~2/3 total). (*C*) Location of place field centroids. Colors denote vertical position. (D) Three-dimensional heat plots of place field orientation for the three maze configurations, ordered as in (B) and (C). Note concentration around horizontal axes for the arena and along the three axes of the aligned and tilted mazes. (E) Graphs show proportion of total fields oriented roughly parallel to each possible maze axis. Red lines show the 1^{st} 50^{th} and 99^{th} percentile of a shuffle distribution. The normalized ratio of XYZ to ABC oriented fields is given as well as the probability of observing this value by chance (see Methods).

Place fields were elongated in all dimensions

Place fields were larger in the two lattice mazes (arena, aligned & tilted median volume: 1065, 1332 & 1535 cm^3, $\chi^2(2) = 63.12$, $p < .0001$, $\eta_p^2 = .04$, K-W; arena vs aligned & arena vs tilted, $p < .0001$) and slightly larger in the tilted than aligned lattice (aligned vs tilted, $p = .021$; Fig. S4D). However, place field diameter varied very little between mazes with only a small, albeit significant, difference between the arena and tilted lattice (arena, aligned & tilted enclosing diameter: 0.65, 0.67 & 0.68m, $\chi^2(2) = 7.3$, $p = .0255$, $\eta_p^2 = .004$, K-W; arena vs aligned & aligned vs tilted, $p > .35$, arena vs tilted, p = .020, Fig S4E). Place fields in all conditions were slightly elongated, with elongation indices (see supplementary methods) that deviated significantly from 1 (arena median elongation: 1.65, Z = 22.81, $p < .0001$, U3 = 0; aligned median elongation: 1.86, Z = 21.29, $p < .0001$, U3 = 0; tilted median elongation: 1.86, Z = 17.29, $p < .0001$, U3 = 0, WSR, Fig. S5A-B). It is unlikely these effects were due to inhomogeneous sampling (Fig. S9). Field heights were bimodal in the aligned lattice, suggesting that vertically elongated fields were longer than horizontally elongated ones (Fig. S5D-E). Place field elongation in the lattice mazes was weakly but significantly positively correlated with field centroid distance from maze center (Fig. S5F).

In the square arena place fields were inhomogeneously distributed ($\chi^2(5) = 918.1$, $p < .0001$, Chi-square test of expected proportions, Fig. 2D) and its axis ratio (total XYZ fields - total ABC fields / sum of these) was significantly greater than zero (observed ratio: 0.65, shuffle 1st & 99th percentile ranks: -0.07 & 0.01) indicating that significantly more fields were oriented parallel to the XYZ axes than ABC axes. Closer inspection revealed that only the horizontal X and Y-axes were represented at an above chance level (X & Y: 31 & 32% of fields, chance 99th percentile: 12.5%, Fig. 2E) and that the fields aligned with these axes were of a similar length ($\chi^2(1) = 0.01$, $p = .97$, $\eta_p^2 < .0001$, K-W).

In the aligned lattice fields were also inhomogeneously distributed ($\chi^2(5) = 152.2$, $p <$ .0001, Chi-square test of expected proportions, Fig. 2D) and its axis ratio was again

significantly greater than zero (observed ratio: 0.39, shuffle 1st & 99th percentiles: -0.072 & -0.001). In this maze only the X, Y and Z-axes were represented at an above chance level (X, Y & Z: 19, 17 & 20% of fields, chance 99th percentile: 12.5%, Fig. 2E) and to an equal degree ($\chi^2(2) = 5.0$, $p = .08$, Chi-square test of expected proportions). However, the fields aligned with these axes differed in length (median length, X, Y & Z: 64.3, 57.9 & 78.2 cm, $\chi^2(2) = 26.8$, $p < .0001$, $\eta_p^2 = .079$, K-W) and post-hoc tests confirmed that fields aligned with the Z-axis were significantly longer (X vs Z & Y vs Z, $p < .009$, X vs Y, $p = .074$).

Lastly, fields in the tilted lattice took on a different non-random distribution ($\chi^2(5) = 27.7$, $p < .0001$, Chi-square test of expected proportions, Fig. 2D) with an axis ratio significantly less than zero (observed ratio: -0.21, shuffle 1st & 99th percentiles: -0.072 & -0.001) indicating that significantly more fields were oriented parallel to the ABC axes than XYZ axes. In line with this only the A, B and C-axes were represented at an above-chance level (A, B & C: each 16% of fields, chance 99th percentile: 12.5%, Fig. 2E) and these fields were all of a similar length ($\chi^2(2) = 0.18$, $p = .91$, $\eta_p^2 < .0001$, K-W). For all three mazes an independent approach also confirmed that field elongation was best described as parallel to each maze's axes (see supplementary results, Fig. S6).

Spatial coding was less accurate along the vertical dimension

If fields were larger along a specific dimension, firing rate maps would be more highly autorcorrelated in this dimension (Fig. S8A-B). In the aligned lattice, autocorrelation values indeed differed between the three axes ($F(2, 26896) = 676.7$, $p < .0001$, $\eta_p^2 = 0.048$) with a significant interaction between distance and axis ($F(40, 26896) = 18.8$, $p < .0001$, $\eta_p^2 = 0.027$) due to higher correlations in the Z-axis (X, Y & Z, mean correlation: 0.165, 0.171 & 0.228; X vs Z and Y vs Z, $p < .0001$, X vs Y, $p = .018$). In the tilted lattice correlation values differed between the A, B and C axes ($F(2,17000) = 22.7$, $p < .0001$, $\eta_p^2 = 0.003$) with an interaction between distance and axis ($F(40,17000) = 2.23$, $p < .0001$, $\eta_p^2 = 0.005$) although

these relationships are associated with small effect sizes. In contrast to the aligned lattice no one axis was associated with higher correlations than the others: instead, the A-axis was associated with slightly smaller correlations (A, B & C, mean correlation: 0.149, 0.161 & 0.160; A vs B and A vs C, $p < .0001$, B vs C, $p > .99$, pairwise comparisons with Bonferroni correction). These effects can be seen in Fig. 3B. Similar effects were obtained using the median overall central component of autocorrelograms (Fig. S8C) and using an independent approach to assess the binary morphological connectivity of lattice firing rate maps (Fig. S8D). Down-sampling trajectory data to account for the horizontal bias in animals' movements confirmed that this bias does not account for these effects (Fig. S9).

To explore this reduced encoding resolution effect further we also looked at the spatial information content along each ratemap axis by calculating the spatial information content after projecting maps onto the Cartesian planes. If fields were larger or if firing was more diffuse along one dimension, place fields would appear larger in slices along the orthogonal axes, resulting in a lower spatial information score (see Fig. S8A-B for an example). The spatial information exhibited by place cells in the aligned lattice did differ along the three axes (median proportion of total spatial information in X, Y & Z slices: 0.308, 0.310, 0.387, $\chi^2(2) = 153.3$, $p < .0001$, $\eta_p^2 = .119$, FT) with horizontal slices along the Z-axis demonstrating the greatest spatial information (X vs Z & Y vs Z, $p < .0001$, X vs Y, $p > .99$). This was not the case in the tilted lattice (median proportion of total spatial information in A, B & C slices: 0.332, 0.333, 0.335, $\chi^2(2) = 1.4$, $p = .498$, $\eta_p^2 = .001$, FT). These effects can be seen in Fig. 3C. Equivalent effects were also observed when using mutual information (data not shown). As before, down-sampling ruled out horizontal movement bias as an explanation for these effects (Fig. S9).

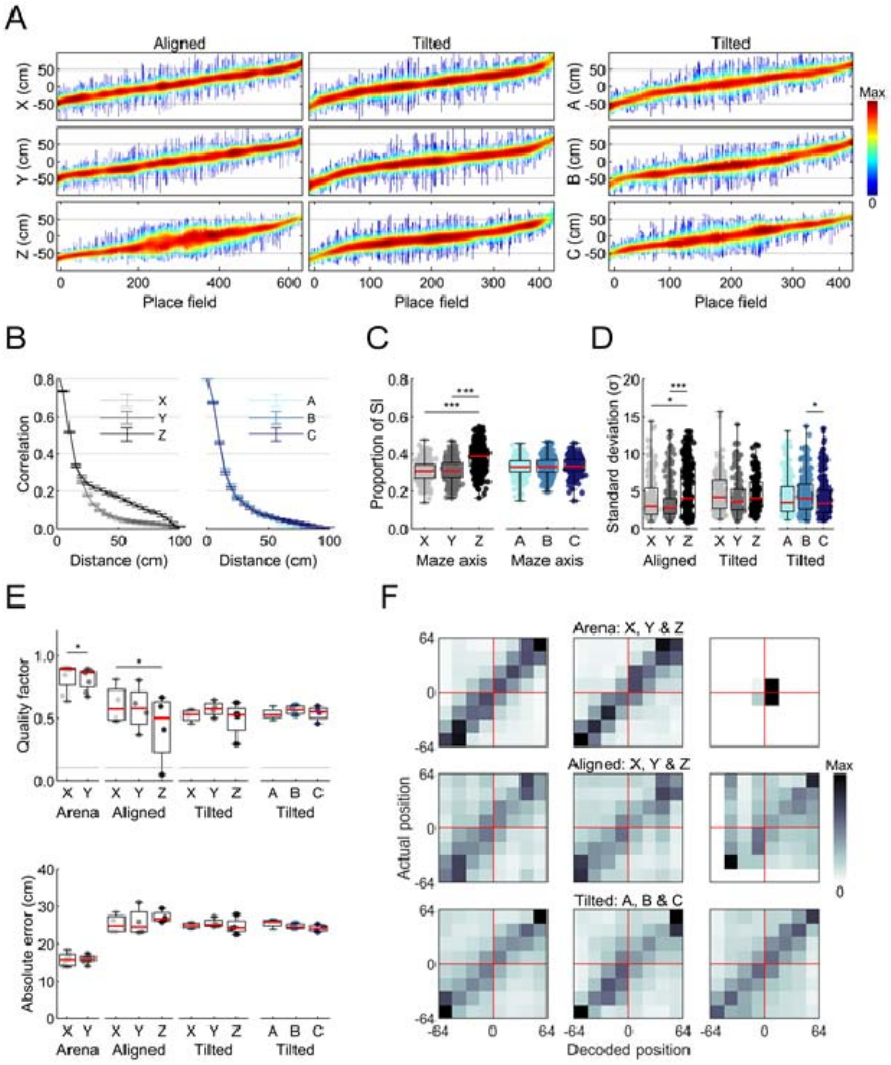

Figure 3: Spatial information in three dimensions. (*A*) The span and normalized activity of every recorded place field in the lattice mazes. Vertical lines represent place fields, ordered along the x-axis by their position relative to the lattice central node. Line color represents normalized firing rate. (*B*) The mean and SEM autocorrelation found for all place cells in the aligned lattice (left) and tilted lattice (right) at increasing distances or spatial lag. Correlations at low distances are high along all axes, however, correlations at longer distances remain higher for longer along the Z axis of the aligned lattice. (*C*) For every cell we generated three 2-dimensional maps by taking the mean along each axis of the 3-dimensional firing rate map. Next we calculated the spatial information content of each map and shown here is the proportion of total spatial information found per projection for the aligned lattice (left) and tilted lattice (right). In the aligned lattice spatial information content is significantly higher when data are projected onto an X, Y plane, suggesting that place cell firing is more precise in these axes. (*D*) The standard deviation of orthogonal 1-dimensional Gaussians fitted to place fields in each lattice maze. (*E*) We decoded the position of animals in each environment through Bayesian methods using the activity of place cells. Top: the quality factor (decoding accuracy relative to chance) of decoded trajectories in each axis. A quality of 0.1 (grey line) is generally considered acceptable. Bottom: the same data as above but showing the actual error in cm for each axis. (*F*) Plots showing decoding accuracy as a function of position along each axis in the open field (top row), aligned lattice (middle row) and tilted lattice (bottom row). Rows are sum normalized, rows or columns with a total probability less than .01 are not shown. Perfect decoding would result in a dark diagonal band in each

plot. Positions are relative to the central node of the lattice mazes or centroid of the open field (red lines).

To investigate this reduced vertical resolution at the level of individual place fields we found the three orthogonal 1D Gaussians (parallel to the Cartesian axes) that best described each place field. In the aligned lattice these Gaussians differed in terms of their standard deviation (median X, Y & Z s.d.; 3.0, 2.7 & 4.1, $\chi^2(2) = 15.4$, $p = .0004$, $\eta_p^2 = .023$, K-W) with the vertical Gaussian (parallel to the Z-axis) best described by a larger standard deviation (X vs Z & Y vs Z, $p < .02$, X vs Y, $p > .92$). By contrast, fields in the tilted lattice could be adequately described by three Gaussians with equivalent standard deviation (median X, Y & Z s.d.; 4.2, 3.6 & 4.1, $\chi^2(2) = 5.0$, $p = .08$, $\eta_p^2 = .008$, K-W). However, the same analysis repeated with Gaussians parallel to the axes of the tilted lattice revealed a small but significant difference between the B and C axes, although this was accompanied by a small effect size (Median A, B & C s.d.; 3.5, 4.1 & 3.4, $\chi^2(2) = 7.5$, $p = .023$, $\eta_p^2 = .009$, K-W; A vs B & A vs C, $p > .23$, B vs C, $p = .02$). These effects can be seen in Fig. 3A & D. An independent approach also confirmed that place field activity was broader along the Z-axis of the aligned lattice (Fig. S8E).

Next, we investigated whether this decreased specificity along the vertical dimension might affect the positional accuracy of the information carried by place cells. To test this we used Bayesian decoding to reconstruct an animal's position during a recording session using only the activity of recorded place cells. In total we decoded 9 arena sessions (2 rats, median, min & max total place cells: 37, 29 & 52), 5 lattice maze sessions (1 rat, median, min & max total place cells: 32, 29 & 52) and 4 tilted maze sessions (1 rat, median, min & max total place cells: 44, 39 & 47). In each, the accuracy of decoding exceeded the 95th percentile of decoding performed on shuffled data. Furthermore, to quantify decoding accuracy in each dimension we computed a quality factor, where the decoded trajectory was compared to the accuracy of a constant value (see supplementary methods). A quality factor of 0.1 is generally used as a cut-off for acceptable decoding accuracy (11, 12). In the open

field session the quality of decoding was equally high for both the X and Y axes (median X & Y quality: 0.89 & 0.87; $\chi^2(1) = 2.78$, $p = .096$, $\eta_p^2 = .15$, FT). However, in the lattice maze decoding quality differed between the three available axes (median X, Y & Z quality: .50, .54 & .41; $\chi^2(2) = 8.40$, $p = .015$, $\eta_p^2 = .56$, FT) with the Z-axis decoding at a significantly lower quality than the X, but equivalent to the Y-axis (X vs Y & Y vs Z, $p > .17$, X vs Z, $p = .013$). In the tilted lattice decoding was equally high along all possible axes (median X, Y & Z quality: .53, .57 & .52; $\chi^2(2) = 3.5$, $p = .17$, $\eta_p^2 = .29$, FT; median A, B & C quality: .52, .57 & .55; $\chi^2(2) = 4.5$, $p = .11$, $\eta_p^2 = .38$, FT). These effects can be seen in Fig. 3E. Closer inspection of the decoded trajectories also revealed that decoding was more accurate at the edges of both lattice mazes (Fig. 3F).

Discussion

This experiment investigated how hippocampal place cells represent three-dimensional, volumetric space in rats, which are predominantly surface-travelling animals. The aim was to see whether all three dimensions would be represented equally, as they are in freely flying bats, implying a volumetric map of space. We used three-dimensional lattice environments where the rats were free to move in any direction, restricted only by the underlying structure of the environment. In one setting the lattice structure was aligned with gravity and in the other it was tilted, enabling us to disentangle restrictions due to gravity from restrictions due to maze structure. We found that place fields packed the lattice space with ovoid fields, in a similar manner to bats, indicating a volumetric map. However the fields were slightly elongated along the maze axes. This was more pronounced in the vertical dimension for the aligned lattice, indicating an interaction between the effects of structure and gravity on place fields. Taken together with previous findings, this suggests that the hippocampal map of three dimensional space is not fixed but is flexibly shaped by environment structure, perhaps via the movement constraints/affordances it provides. Below, we discuss the findings that lead to this conclusion, and its implications.

When the lattice was aligned with gravity we found that rats explored using a “layer strategy” in which they fully explored one level before moving to the next, meaning far fewer vertical movements than horizontal ones – this replicates previous findings and is consistent with the notion that animals will execute the easier parts of a multi-stage journey first (10). When the maze was tilted, all three principal axes became sloped relative to gravity and thus equally easy/hard to traverse, and the layer strategy disappeared. We also found that rats spent more time in the lower part of the mazes.

In both maze alignments, we found that place fields were distributed evenly throughout the volume of the lattices and had broadly similar properties in vertical vs. horizontal dimensions. They were larger in volume than fields in the open-field arena,

suggesting that the hippocampal representation of space scales according to environment demands. This observation supports the multiscale spatial representation proposed by Geva-Sagiv et al. (13). Furthermore, we also observed the same sublinear relationship between environment and place field size as that study; place field size did not scale linearly with the environment but instead at a reduced rate, an effect which has also been reported previously in rats (14). Oddly however, we did not observe a significant increase in the number of place fields exhibited per cell in the lattice maze environments.

We next looked at the structure of place fields in the different dimensions, finding that place fields tended to be elongated, as has been generally seen (10, 11). Elongation did not occur in every direction but was almost always in the direction of the maze axes/boundaries. Two related explanations for why this might occur present themselves. One is that the maze boundaries, represented by the termination of the cross-bars, serve to anchor place fields in a similar way to walls and edges in a flat environment, possibly via boundary cells found in the subiculum (12) and medial entorhinal cortex (13). These have been shown to respond to both walls and edges (15, 16) and are able to “reset” the spatial firing of entorhinal grid cells (17). Since the effect of anchoring falls off with distance due to accumulating path integration error, fields should tend to be narrower in the direction orthogonal to the nearest boundary, for which distance to the wall is small, and elongated in the direction that runs between the two more distant boundaries. The other explanation is that perhaps fields tend to be elongated in the direction more frequently traversed by the animals, or that is traversed for a longer continuous time. Since animals can spend relatively little time running directly towards or away from a boundary, but much time running back and forth along it, synaptic plasticity would have more opportunity to “grow” fields along the direction of travel. A similar argument could explain elongation along maze axes, although rats rarely moved vertically in the aligned lattice yet fields were still elongated along this axis. In the present experiment we did not investigate this further by rotating the axes relative to the boundaries, but this would be an interesting task for future experiments.

We next looked at whether field elongation was greater in the vertical dimension. Previous research in rats on vertical surfaces found the vertical dimension to be represented differently, although the exact nature of this difference depended on the movement patterns. When the rats climbed on pegs but remained oriented mainly horizontally then place fields were elongated vertically (6), whereas when the animals climbed by clinging to chicken wire and were thus aligned with the wall then place fields were sparser, but no longer vertically elongated (7). In a study of flying bats, fields were not different from spherical (18). In the present experiment we found an increase in place field elongation in the vertical dimension, which was also represented less stably: however this was only when the maze was aligned with gravity, and not when it was tilted. The aligned configuration is the one that induced differential movement patterns, with freer movement in x-y than in z. Putting all these experiments together, the hypothesis emerges that place fields have less resolution in a dimension in which the animal does not freely travel in the direction of its body axis. This might occur if the distance-tracking process is not uniform in all directions but works best in the direction of travel.

The heterogeneity of findings in the different mazes points to a fundamental conclusion which is that there is not a fundamental, holistic map of space that permeates three-dimensional space and is sampled by the animal as it moves through the space over various surfaces. This is because no unitary map structure could account for field elongation on the pegboard, field sparsity on the chicken-wire “cling wall” and rather, it seems that a different kind of place cell representation is recruited depending on environment structure and perhaps task demands.

Our findings of a volumetric place cell map agree not only with the data from bats but also from recent neuroimaging work in humans, suggesting the encoding resolution for movement along a vertical axis in a lattice maze does not differ greatly from horizontal (19). However behavioral experiments suggest a subtle difference, with an advantage in memory for horizontal as compared to vertical space (4). More recent evidence suggests that people

362 wrongly estimate the position of objects in a well-known building, giving the overall effect of a
363 vertically elongated but horizontally contracted spatial representation (20) which is in
364 agreement with our finding of increased elongation along the vertical dimension (but see
365 (21). The path which participants use to explore a building has also been shown to play a
366 crucial role; people who explore a building by mainly vertical paths were better at recalling
367 the positions of vertically arranged objects than people who explored the same building by
368 mainly horizontal paths (22) supporting the importance of environment affordances in the
369 development of spatial representations.

370 In this paper we have shown that surface-dwelling animals such as rats do have a
371 volumetric representation of space and that this representation exhibits many of the same
372 characteristics as two-dimensional representations. Place fields are elongated parallel to the
373 primary axes of every environment with a slight bias towards vertical elongation and spatial
374 coding and stability are significantly reduced along this dimension, suggesting that these
375 animals may not encode the vertical dimension with equal accuracy. Future research will
376 need to investigate these effects in volumetric animals such as flying bats to determine if
377 spatial maps share a common organization across species or if separate neural mechanisms
378 exist in volumetric animals. Our results point to an important effect of environmental
379 affordances, evidence of which can be seen in other spatial mapping literature. However,
380 more research is needed to tease apart the relationship between affordances, geometry,
381 gravity and behavioral sampling. This could look to combine recordings with behavioral
382 training, to increase sampling of the more difficult vertical dimension. Our results, combined
383 with those from recent experiments on the head direction system (23, 24) suggest that the
384 rodent spatial navigation network may be far better at mapping three-dimensional space
385 than previously thought. This confirms the relevance of rodents such as rats in studying
386 these representations and undermines the view that volumetric animals such as bats are
387 necessary for these experiments. It also opens up new avenues of research and raises
388 questions regarding other spatial cells such as grid and boundary cells in the Subiculum and

389 medial entorhinal cortex. It is difficult to draw direct parallels between grid and place cells,
390 but the strong spatial representations we have observed in place cells points to a strong
391 possibility of distinct spatial representations of volumetric space by grid cells which have yet
392 to be explored.
393

Methods

Statistics and figures

Statistics and data analysis were performed using Matlab (R2018a, The MathWorks, Inc.) or SPSS (IBM SPSS statistics 25). If data were found to deviate significantly from a normal distribution (Matlab functions *lillietest*, *skewness*, *kurtosis*) we utilised non-parametric tests such as the Wilcoxon signed rank test (WSR, Matlab function *ranksum*), permutation-F test, Kruskal-Wallis (K-W, Matlab function *kruskalwallis*) or Friedman test (FT, Matlab function *friedman*) and post-hoc tests compared average ranks (Matlab function *multcompare*, Bonferroni correction). Otherwise, we used parametric tests and post-hoc tests compared population means (Matlab function *multcompare*, Bonferroni correction). Except in the case of multivariate comparisons where we sought to determine any interaction effects, then we employed generalized linear models using SPSS. Where possible we report effect sizes for each test: partial eta squared (η_p^2, proportion of variance in the DV explained by an IV) for K-W, FT and ANOVAs; Cohen's U3 (U3, fraction of values in group 1 less than those in group 2 or the test value in a one-sample test) for WSR; odds ratio (OR, the ratio of the odds of an event occurring in one group to the odds of it occurring in another group) for Chi-square tests of equal proportions. Unless otherwise stated all statistical tests are two-tailed. In all figures * = significant at the .05 level, ** = significant at the .01 level, *** = significant at the .001 level. For all box plots red lines denote the sample median, boxes denote interquartile range, whiskers span the full range of the data and markers represent individual data points.

Subjects

Thirteen animals were used for single unit electrophysiological recording (9 in the lattice, 4 in the diagonal lattice), at which point they weighed approximately 400–450 g. All animals were housed for a minimum of 8 weeks in a large (2150mm x 1550mm x 2000mm)

cage enclosure, lined on the inside with chicken wire. This was to provide the rats with sufficient experience climbing in a three-dimensional environment. Inside this cage the rats were also given unlimited access to a miniature version of the lattice maze. This was composed of similar lattice cubes (55 x 55 x 55) but with a slightly smaller spacing (11cm) and was oriented to match the experimental version appropriate to the rats (i.e. rats recorded in the aligned lattice were exposed to a miniature aligned lattice, rats recorded in the tilted lattice were exposed to a miniature tilted lattice). Animals were housed individually in cages after surgery and there they were given access to a hanging hammock or climbable nest box for continued three-dimensional experience.

The animals were maintained under a 12□hr light/dark cycle and testing was performed during the light phase of this cycle. Throughout testing, rats were food restricted such that they maintained approximately 90% (and not less than 80%) of their free-feeding weight. This experiment complied with the national [Animals (Scientific Procedures) Act, 1986, United Kingdom] and international [European Communities Council Directive of November 24, 1986 (86/609/EEC)] legislation governing the maintenance of laboratory animals and their use in scientific experiments.

Electrodes and surgery

A combination of Axona (MDR-xx, Axona, UK) and tripod design (Kubie, 1984) microdrives were used (rats 750, 770, 775 Kubie drives, all other rats Axona drives). Drives supported four or eight tetrodes, each of which was composed of four HML coated, 17 mm, 90% platinum 10% iridium wires (California Fine Wire, Grover Beach, CA). Tetrodes were threaded through a thin-walled stainless steel cannula (21 Gauge Hypodermic Tube, Cooper's Needle Works Ltd., UK). Electrode tips were gold plated (Non-Cyanide Gold Plating Solution, Neuralynx, MT) in order to reduce the impedance of the wire from a resting impedance of 0.7–0.9 MΩ to a plated impedance in the range of 180–300 kΩ (200 kΩ being the target impedance).

Microdrives were implanted using standard stereotaxic procedures under isoflurane anaesthesia. Hydration was maintained by subcutaneous administration of 2.5 ml 5% Hartman's solution and 1 ml 0.9% saline. Animals were also given an anti-inflammatory analgesia (small animal Carprofen/Rimadyl, Pfizer Ltd., UK) subcutaneously. Electrodes were lowered to just above the CA1 cell layer of the hippocampus (-3.5 mm AP from bregma, ±2.4 mm ML from the midline, ~1.5 mm DV from dura surface). The drive assembly was anchored to the skull screws and bone surface using dental cement. Animals recovered in a chamber, heated to body temperature. Following this, at least one week of recovery time passed before animals were screened for cells. During this week, the animals' food was tapered from free feeding to the pre-surgery level of restriction.

Apparatus

All experiments were conducted in the same room under moderately dimmed light conditions. A detailed description of the room and apparatus can be found in supplementary methods, Fig. S1 and Fig. 1A. Briefly, we used three main pieces of experimental apparatus; a square open field environment ('arena'), a cubic lattice composed of horizontal and vertical climbing bars ('aligned' lattice) and the same lattice rotated to stand on one of its vertices ('tilted' lattice). Rats were recorded freely foraging in the arena for randomly dispersed flavoured puffed rice (CocoPops, Kelloggs, Warrington, UK) and foraging in the lattice maze for malt paste (GimCat Malt-Soft Paste, H. von Gimborn GmbH) affixed to bars of the lattice.

Recording setup and procedure

A detailed description of the recording setup used can be found in supplementary methods. Briefly, single unit activity was observed and recorded using a custom built 64-channel recording system (Axona, St. Albans, UK) and a wireless headstage (custom 64-channel, W-series, Triangle Biosystems Int., Durham, NC) mounted with infrared LEDs. Five infrared sensitive CCTV cameras (Samsung SCB-5000P) tracked the animal's position at all times (see Trajectory reconstruction section of supplementary methods for more details). For

experimental sessions, rats were recorded for a minimum of 18 minutes in the arena, followed by a minimum of 45 minutes in one configuration of the lattice and a further minimum 16 minutes in the arena.

Behavioural analyses

Using smoothed and interpolated 3D reconstructed position data we detected when the rat crossed from one 16cm^3 lattice maze cubic element to another along each axis. As our maze sessions vary in length these values are expressed as a rate per second. In a more sensitive approach, we calculated the instantaneous three-dimensional heading of the animal as the normalised change in position:

$$\hat{u} = \frac{\vec{u}}{||\vec{u}||}$$

where;

$$\vec{u} = (\Delta_X(t), \Delta_Y(t), \Delta_Z(t))$$

and;

$$||\vec{u}|| = \sqrt{\Delta_X(t)^2 + \Delta_Y(t)^2 + \Delta_Z(t)^2}$$

this gives a unit vector representing the animal's heading at time *t*. We then projected these vectors on to a unit sphere and extracted position data falling within regions on the surface of the sphere corresponding to the intersection of the sphere and the axes of interest; the Cartesian X (Pitch = 0°, Azimuth = 0° & 180°), Y (Pitch= 0°, Azimuth = 90° & 270°), Z (Pitch,= ±180°, Azimuth = 0°) axes and the diagonal lattice maze relative A (Pitch = ±35.26°, Azimuth = -60° & 120°), B (Pitch = ±35.26°, Azimuth = 60° & -120°) and C (Pitch = ±35.26°, Azimuth = -180° & 0°) axes. The regions were equivalent to 60° conic sections centred on each respective axis in one direction from the origin. For each axis we combined the two corresponding directional regions. The length of time spent moving along each of these axes

was calculated as the number of position samples falling along each of these axes multiplied by the sampling rate of the system. For this analysis we used only data when the animal was travelling at a speed >20cm/s. The average speed of movement along each axis was calculated separately as the total distance travelled in each axis divided by the total session time.

We also calculated the kernel smoothed density estimate of these spherical points using a Von Mises–Fisher distribution. Briefly, the Gaussian used was defined as:

$$g(x) = \frac{\frac{e^{(-0.5\left(\frac{x}{\sigma}\right)^2)}}{\sqrt{2\pi(\sigma)}}}{1/\sigma}$$

where x was defined as the inverse cosine of the inner dot product between each vector point and points across a sphere's surface (Matlab function *sphere*) and σ was the standard deviation of the Gaussian, which was set to 10. In this way, the resulting three-dimensional heat plots give a density estimate of points on the sphere, where density is estimated as the sum of the Gaussian weighted distances (along the surface of the sphere) to every data point.

For a measure of three-dimensional thigmotaxis we calculated the total length of time spent in the inner and outer half volumes of the lattice – the inner half being an approximately 77cm^3 cube centred on the centre of the lattice. For the diagonal lattice, this central cube was rotated to match the geometry of the maze. Dwell time ratio was calculated as the ratio of these two values for each session. For the square arena environment, we omitted the Z-dimension, instead the inner half was defined as the square region with half the surface area of the arena centred on the middle of the maze.

To determine if the rats displayed a bias in their occupancy of 3D space, we also calculated the length of time the rats spent in the top and bottom of the two lattice mazes.

For this we categorised data as either above the centre node of the lattice (top) or below it (bottom). Dwell time ratio was calculated as the ratio of these two values for each session. As a measure of exploration coverage, for each session we calculated the proportion of lattice maze nodes (climbing bar intersections) enclosed by the convex envelope of that session's position data. For later place field analyses we also estimated the practical volume of the lattice mazes and arena maze as the average volume of these convex hulls.

Firing rate maps

Three-dimensional volumetric firing rate maps were constructed using a similar approach to that reported previously (25). This procedure is outlined in greater detail in supplementary methods.

Place cell criteria

A cluster was classified as a place cell if it satisfied the following criteria in the session with the greatest number of spikes: i) the width of the waveform with the highest amplitude was >250 μs, ii) the mean firing rate was greater than 0.1 Hz but less than 10Hz and iii) the spatial information content was greater than 0.5 b/s. Spatial information content was defined as:

$$information\ content = \sum P_i(\frac{R_i}{R})log_2(\frac{R_i}{R})$$

where i is the voxel number, P_i is the probability for occupancy of voxel i, R_i is the mean firing rate for voxel i, and R is the overall average firing rate (26). In combination with these parameters we also manually refined the resulting place cell classification in order to resolve false positives and negatives.

Isolating place fields

Unless otherwise stated, all analyses were performed on the unsmoothed firing rate maps produced using the above method. When detecting place fields, we looked for areas of

more than 64 contiguous voxels (a cube with side length 4 voxels, equivalent to 8000 cm^3 or 20×20×20 cm) with a firing rate greater than 20% of the maximum value in the rate map. Contiguity was defined as a three-dimensional 18-connected neighbourhood, which includes all voxels sharing an edge or face but not only a vertex. This was calculated using the Matlab function *bwlabeln*. Additionally, a place field had to be visited more than 5 times, where a visit was defined as 1 second of contiguous time spent within the place field convex hull.

Place field features

We then extracted the main features of these place fields (Matlab function *regionprops3*). These included the convex volume, which was defined as the number of voxels contained within the smallest convex polygon that could contain the place field and position, which was defined as the centroid, or centre of mass of the field's voxels. We also extracted the field's orientation and principal axes, which were defined as the orientation and major axes of an ellipsoid with the same normalized second central moments as the field region, calculated using its eigenvectors. We also extracted the Cartesian height and width of the fields, defined as the total length of the field region when projected on to the X, Y and Z-axes respectively. We calculated the elongation index of the principal axes as:

$$Elongation = \frac{P1}{0.5(P2 + P3)}$$

where $P1$, $P2$ and $P3$ are the principal axes from largest to smallest respectively. This gives a measure of the curvature of the place field; large elongation values represent elongated fields while a value of 1 would represent a sphere. In the case of the arena elongation was calculated using the first two largest principal axes (P1/P2). This is because animals were unable to move vertically, trajectories and ratemaps in this environment are flattened vertically and the Z-axis makes little sense from an analytical standpoint. As an additional

559 geometric measure, independent of the axis lengths, we also calculated the sphericity of
560 each place field's convex hull, sphericity was defined as:

$$sphericity = \frac{\pi^{\frac{1}{3}}(6V)^{\frac{2}{3}}}{A}$$

561 where V is the volume of the place field and A is its surface area. A sphericity of 1 would
562 represent a sphere and any deviation from a sphere would result in a value lower than this.

563 *Field orientation*

564 To determine if fields were oriented in three-dimensions along one or more arbitrary
565 axes we projected the place field eigenvectors (and their antipodal equivalents) on to a unit
566 sphere. Using a similar analysis as the one described for position data, we then extracted
567 the number of fields falling within regions on the surface of the sphere corresponding to the
568 intersection of the sphere and the axes of interest; the Cartesian XYZ axes and the lattice
569 maze relative ABC axes. These regions are equivalent to ~60° conic sections centred on
570 each respective axis in one direction from the origin, thus for each axis we combined the two
571 corresponding directional regions (which in this case are merely mirror images). As fields
572 were observed to fall in alignment with the XYZ axes in the lattice maze and the ABC axes in
573 the diagonal lattice we computed an 'axis ratio' for comparison. This was defined as:

$$axis\ ratio = (XYZ - ABC)/(XYZ + ABC)$$

574 where XYZ is the total number of fields parallel to the X, Y and Z axes and ABC is the same
575 for the A, B and C axes. For comparison we randomly distributed 1000 points across the
576 surface of a sphere 1000 times and recomputed the above values. If the number of fields
577 aligned with a particular axis exceeded the 99th percentile of this shuffled distribution it was
578 considered to be significantly overrepresented. If the axis ratio of a maze exceeded the 99th
579 percentile of the ratios obtained in the shuffle it was defined as significantly deviating from 0
580 (no axis bias of any kind) and the sign of the observed ratio was taken as the direction of

581 significance (i.e. >0 = bias towards XYZ, <0 = bias towards ABC). Next, we calculated the
582 Von Mises–Fisher kernel smoothed density estimate of these place field vectors across the
583 sphere's surface (as described in Behavioural analyses). These 3D spherical maps are
584 presented in the main text for visualisation only (Fig. 1 & 2).

585 *Bayesian decoding*

586 To further test for any anisotropy that might not be apparent or detectable in the firing
587 fields of place cells, we also performed Bayesian position decoding (see supplementary
588 data) on sessions in which more than 25 place cells were simultaneously recorded using the
589 method outlined by Zhang et al. (27). We simultaneously recorded a sufficiently large sample
590 of place cells in a total of 9 arena sessions (Median, min & max total place cells: 37, 29 &
591 52), 5 lattice maze sessions (Median, min & max total place cells: 32, 29 & 52) and 4 tilted
592 maze sessions (Median, min & max total place cells: 44, 39 & 47).

593

Acknowledgments

This work was supported by a grant from Wellcome (103896AIA) to K.J.

Author contributions

K.J. conceived the study and obtained funding, S.R., R.G. and K.J. designed the protocol, R.G., S.J-A., K.M., A.L. and S.R. performed surgeries and recordings, R.G analyzed data. All authors interpreted data and discussed results. R.G. and K.J. wrote the manuscript. All authors commented and edited the manuscript.

Competing financial interests

KJ is a non-shareholding director of Axona Ltd.

References

1. Tolman EC (1948) Cognitive maps in rats and men. *Psychol Rev* 55(4):189–208.

2. O'Keefe J, Nadel L (1978) *The Hippocampus as a Cognitive Map* (Clarendon Press, Oxford).

3. Jeffery KJ, Wilson JJ, Casali G, Hayman RM (2015) Neural encoding of large-scale three-dimensional space—properties and constraints. *Front Psychol* 6. doi:10.3389/fpsyg.2015.00927.

4. Jeffery KJ, Jovalekic A, Verriotis M, Hayman R (2013) Navigating in a three-dimensional world. *Behav Brain Sci* 36(05):523–543.

5. Finkelstein A, Las L, Ulanovsky N (2016) 3D maps and compasses in the brain. *Annu Rev Neurosci* 39:171–196.

6. Hayman R, Verriotis MA, Jovalekic A, Fenton AA, Jeffery KJ (2011) Anisotropic encoding of three-dimensional space by place cells and grid cells. *Nat Neurosci* 14(9):1182–8.

7. Casali G, Bush D, Jeffery KJ (2019) Altered neural odometry in the vertical dimension. *PNAS*:pii: 201811867.

8. Gibson JJ (1986) *The Ecological Approach to Visual Perception* (Lawrence Erlbaum Associates).

9. Yartsev MM, Ulanovsky N (2013) Representation of Three-Dimensional Space in the Hippocampus of Flying Bats. *Science* 340(6130):367–72.

10. Jovalekic A, et al. (2011) Horizontal biases in rats' use of three-dimensional space. *Behav Brain Res* 222(2):279–288.

11. Saleem AB, Ayaz A, Jeffery KJ, Harris KD, Carandini M (2013) Integration of visual motion and locomotion in mouse visual cortex. *Nat Neurosci* 16(12):1864–1869.

12. Glaser JI, Chowdhury RH, Perich MG, Miller LE, Kording KP (2017) Machine learning for neural decoding. *arXiv:170800909 [q-bioNC]*.

13. Geva-Sagiv M, Las L, Yovel Y, Ulanovsky N (2015) Spatial cognition in bats and rats: from sensory acquisition to multiscale maps and navigation. *Nat Rev Neurosci* 16(2):94–108.

14. Muller RU, Kubie JL (1987) The effects of changes in the environment on the spatial firing of hippocampal complex-spike cells. *J Neurosci* 7(7):1951–1968.

15. Lever C, Burton S, Jeewajee A, O'Keefe J, Burgess N (2009) Boundary vector cells in the subiculum of the hippocampal formation. *J Neurosci* 29(31):9771–9777.

16. Solstad T, Boccara CN, Kropff E, Moser MB, Moser EI (2008) Representation of geometric borders in the entorhinal cortex. *Science* 322(5909):1865–1868.

17. Hardcastle K, Ganguli S, Giocomo LM Environmental boundaries as an error correction mechanism for grid cells. *Neuron* 86(3):827–839.

18. Yartsev MM, Ulanovsky N (2013) Representation of three-dimensional space in the hippocampus of flying bats. *Science (80-)* 340(6130):367–372.

19. Kim M, Jeffery KJ, Maguire EA (2017) Multivoxel Pattern Analysis Reveals 3D Place Information in the Human Hippocampus. *J Neurosci* 37(16).

20. Brandt T, et al. (2015) "Taller and Shorter": Human 3-D spatial memory distorts familiar multilevel buildings. *PLoS One* 10(10):e0141257.

21. Wilson PN, Foreman N, Stanton D, Duffy H (2004) Memory for targets in a multilevel

simulated environment: Evidence for vertical asymmetry in spatial memory. *Mem Cognit* 32(2):283–297.

22. Dollé L, Droulez J, Bennequin D, Berthoz A, Thibault G (2015) How the Learning Path and the Very Structure of a Multifloored Environment Influence Human Spatial Memory. *Adv Cogn Psychol* 11(4):156–162.

23. Page HJI, Wilson JJ, Jeffery KJ (2018) A dual-axis rotation rule for updating the head direction cell reference frame during movement in three dimensions. *J Neurophysiol* 119:192–208.

24. Laurens J, Angelaki DE (2018) The brain compass: A perspective on how self-motion updates the head direction cell attractor. *Neuron* 97:275–289.

25. Leutgeb S, et al. (2005) Independent codes for spatial and episodic memory in hippocampal neuronal ensembles. *Science (80-)* 309(5734):619–623.

26. Skaggs WE, McNaughton BL, Wilson MA, Barnes CA (1996) Theta phase precession in hippocampal neuronal populations and the compression of temporal sequences. *Hippocampus* 6(2):149–172.

27. Zhang K, Ginzburg I, McNaughton BL, Sejnowski TJ Interpreting neuronal population activity by reconstruction: unified framework with application to hippocampal place cells. *JNeurophysiol* 79(2):1017–1044.